ChemComm

COMMUNICATION

View Article Online
View Journal | View Issue

Cite this: *Chem. Commun.*, 2024, **60**, 2026

Received 11th December 2023,
Accepted 20th January 2024

DOI: 10.1039/d3cc06000d

rsc.li/chemcomm

Liquid-crystalline circularly polarised fluorescent emitters with a high luminescence dissymmetry factor†

Xiaoyi Lai,[a] Qihang Zhong,[a] Chen Xiao,[a] Stephen J. Cowling,[c] Pengfei Duan,*[b] Duncan W. Bruce,*[c] Weiguo Zhu[a] and Yafei Wang*[a]

Chiral liquid-crystalline emitters based on 9,9-dimethyl-10-(4-(phenylsulfonyl)phenyl)-9,10-dihydroacridine and a functionalised binaphthol show smectic liquid crystal phases and circularly polarised blue fluorescence with a high luminescence dissymmetry factor $|g_{lum}|$ of 0.13. Solution-processable organic light-emitting diodes (OLEDs) based on the enantiomers were explored.

Circularly polarised light has considerable potential applications in 3D displays, chiral phototransistors, quantum information processing, information encryption and chiral photocatalysis.[1–3] Generally, circularly polarised light is generated by passing unpolarised light successively through a linear polariser and quarter-wave plate, which unfortunately leads to at least a 50% loss in brightness.[4] Thus, it is necessary to develop chiral luminescent systems enabling direct emission of left- or right-handed circularly polarised light, *i.e.* which exhibit circularly polarised luminescence (CPL). The intensity of CPL emission is expressed as the luminescence dissymmetry factor (g_{lum}), defined as $2(I_L - I_R)/(I_L + I_R)$, where I_L and I_R refer to the intensities of left and right CP-emitted light, respectively at the emission maximum; it has a maximum magnitude of 2.[5,6]

While polymeric materials have attracted a good deal of attention, small organic molecules with CPL-activity (CPL-SOMs) have attracted much interest because of their advantages such as defined molecular weight, good repeatability and high purity.[7] Many years ago, Chen *et al.* reported g_{lum} values of $\approx \pm 1.8$ using a commercial poly(fluorene) luminophore dissolved in a chiral nematic glass,[8] after which Woon *et al.* adopted a parallel approach to record g_{lum} values of 1.77 for a coumarin dye, also dissolved in a (different) chiral nematic glass. In these systems, CPL arises from the inherent chirality of the host matrix[9] and there is non-radiative transfer from the excited state of the host to the guest emitter.

More recently, attention has turned to the use of chiral emitters and, for example, Gon *et al.* reported values for g_{lum} = 0.27 for thick, drop-cast films of chiral [2.2]paracyclophanes,[10] while Zinna *et al.* employed phenylene bis-thiophenyl-propynones bearing chiral ancillary chains to produce spin-coated films for which g_{lum} was evaluated to be 0.15.[11]

To this end, many CPL-SOMs have been developed in recent years, especially where CPL is combined with thermally activated delayed fluorescence (TADF).[12,13] However, while good emission efficiencies have been achieved for such CPL emitters, most values of g_{lum} range from 10^{-5} to 10^{-3},[14] lagging far behind those of conjugated polymers and some of the self-organised systems just described.[15,16] Therefore, combining high emission efficiencies and large values of g_{lum} represents a formidable challenge in the design of CPL-SOMs.[17]

As shown by the work of Chen *et al.* and Akagi *et al.*, introducing liquid crystallinity into chiral luminescent materials has been identified as an effective strategy to realise high-efficiency CPL, an approach which continues to attract attention.[18–21] For example, Wu *et al.* reported chiral nematic distyrylbenzenes with a photoluminescence quantum yield (PLQY) of $\approx$74% and a large g_{lum} value of 0.11,[22] while others reported strongly circularly polarised luminescence from films doped with chiral liquid crystals.[23] Similarly, we developed chiral, phosphorescent platinum metallomesogens which, when fabricated into OLED devices, showed external quantum efficiencies (EQE) of above 12% and a high g_{lum} value of 10^{-2}.[13,16,24] However, chiral liquid crystals with $g_{lum} > 10^{-1}$ remain rare.

[a] *Jiangsu Collaborative Innovation Center of Photovoltaic Science and Engineering, Jiangsu Engineering Laboratory of Light-Electricity-Heat Energy-Converting Materials and Applications, School of Materials Science & Engineering, Changzhou University, Changzhou 213164, China. E-mail: qiji830404@hotmail.com*

[b] *CAS Center for Excellence in Nanoscience, CAS Key Laboratory of Nanosystem and Hierarchical Fabrication, National Center for Nanoscience and Technology (NCNST), No. 11 ZhongGuanCun BeiYiTiao, Beijing 100190, P. R. China. E-mail: duanpf@nanoctr.cn*

[c] *Department of Chemistry, University of York, Heslington, York, YO10 5DD, UK. E-mail: duncan.bruce@york.ac.uk*

† Electronic supplementary information (ESI) available: Details of synthesis and characterisation, additional mesophase characterisation data and details of some photophysical properties, in particular those of ***S*-3**. See DOI: https://doi.org/10.1039/d3cc06000d

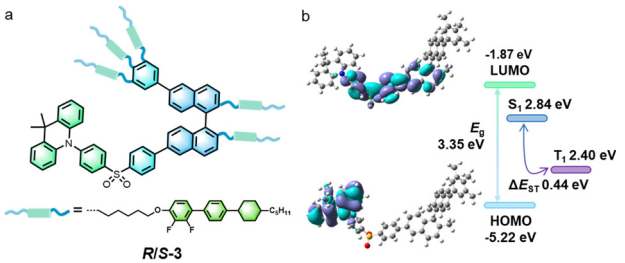

Fig. 1 (a) Structure of the chiral liquid-crystalline emitters and (b) the DFT-calculated HOMO and LUMO distributions.

We now report preparation and photoluminescence properties of the enantiomeric mesogens ***R*/*S*-3** (Fig. 1), which use binaphthol as the chiral group, 9,9-dimethyl-10-(4-(phenylsulfonyl)phenyl)-9,10-dihydroacridine as the luminophore and 2,3-difluoro-4-(heptyloxy)-4′-(4-pentyl-cyclohexyl)-1,1′-biphenyl as the mesogenic fragment. The compounds are prepared as described in the ESI† and were characterised by NMR spectroscopy and TOF mass spectrometry.

Cyclic voltammetry‡ of ***R*-3** in CH_3CN showed a single, irreversible oxidation (Fig. S11, ESI†) at 0.75 V, from which E_{HOMO} was calculated to be −5.10 eV and E_{LUMO} −1.84 eV, using $E_{HOMO} = -(E_{Ox} + 4.8 - E_{Fc/Fc^+})$ and $E_{LUMO} = E_{HOMO} + E_g^{opt}$.[23] Calculation of the geometry and frontier orbitals of ***R*-3** (Gaussian 09, B3LYP, def2SVP basis set) provided further information concerning these new materials (Fig. 1b). The molecule has a distorted molecular geometry, with the acridine and diphenylsulfone fragments being close to perpendicular. The HOMO (−5.22 eV) is localised on the acridine moiety, while the LUMO (−1.87 eV) is mainly distributed over the diphenylsulfone and naphthalene units; calculated energies match well with the electrochemical measurements. The location of the LUMO means that the chiral unit is involved in the luminescence, leading to the potential for relatively high values of g_{lum}. However, while there is good spatial separation between the HOMO and LUMO orbitals in this molecule, the relatively large single-triplet energy difference (ΔE_{ST} = 0.44 eV) suggests a difficult reverse intersystem crossing process.[25]

Using a combination of polarised optical microscopy, differential scanning calorimetry (DSC) and small-angle X-ray scattering (SAXS) (Fig. 2), it was possible to characterise the liquid crystalline behaviour of the materials. Cooling the compound from its isotropic phase led to the formation at 162 °C of a SmA* phase (designated SmA* on account of the chiral nature of the compound, although this has no real impact on the phase itself), which then gave way to a more ordered phase at 134.5 °C, albeit with a rather imperceptible change in texture (Fig. S13, ESI†). SAXS revealed two orders of lamellar reflection were observed in the SmA* phase, with a lamellar spacing of 44.0 Å calculated from the $d(001)$ reflection at $2\theta = 2.0°$. A weak (002) reflection is observed at $2\theta = 3.98°$. Cooling below 134.5 °C leads to a significant change in observed layer spacing and much greater correlation between layers with the observation of four orders of lamellar reflection – $d(001)$ to $d(004)$, with $d(001)$ observed at $2\theta = 0.86°$ corresponding to a spacing of 102.9 Å.

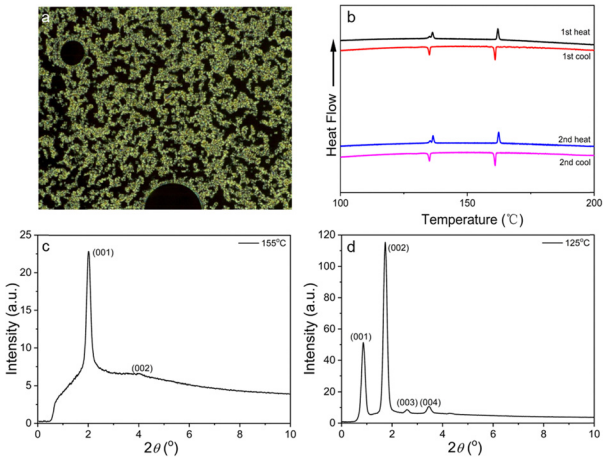

Fig. 2 (a) Optical texture of ***R*-3** in the SmA* phase at 161 °C; (b) DSC curve for ***R*-3**; SAXS diffraction patterns for ***R*-3** (c) in the SmA* phase at 155 °C and (d) in the SmA_2* phase at 125 °C.

The intensity of the $d(002)$ reflection is greater than that of the $d(001)$, implying a bilayer spacing ($d(004)$ is also more intense than $d(003)$) and so the lower-temperature phase is assigned as a bilayer smectic A phase – SmA_2*. Thermogravimetric analysis (Fig. S12, ESI†) shows good thermal stability for ***R*-3** with a decomposition temperature (at 5% weight loss) of 387 °C.

Electronic absorption spectra (toluene, 10^{-5} M) showed absorptions at 283 and 350 nm (Fig. 3a), the former originating from the π–π* transitions of the aryl ring moiety, while the latter can be attributed to the intramolecular charge-transfer (ICT) transition localised on the emission core.[26] Upon photoexcitation at 350 nm, ***R*-3** shows blue emission at 466 nm, with a 14 nm red shift compared to that of the parent emissive acridine-based core.[27] This implies that the binaphthalene moiety has only a small effect on the excited state properties and the broad, structureless emission spectrum suggests that it

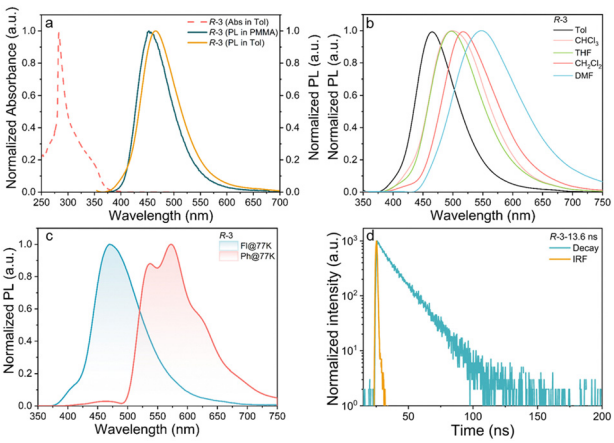

Fig. 3 Photophysical properties of ***R*-3**. (a) Normalised UV absorption (dashed line) and PL spectra in toluene solution (10^{-5} M) and doped in PMMA film (λ_{ex} = 350 nm); (b) PL spectra in different solvents at room temperature; (c) low temperature fluorescence and phosphorescence (delayed 2 ms) spectra in toluene solution; (d) time-resolved emission of ***R*-3** in toluene solution (10^{-5} M) (λ_{ex} = 350 nm).

originates from a charge-transfer (CT) excited state.[28] Large, positive solvatochromism was observed for the solvent-dependent emission spectra (Fig. 3b), further indicative of the strong charge-transfer nature of the excited state. As depicted in Fig. 3a, the PL spectra of ***R*-3** doped in a PMMA film exhibits a small blue shift of 12 nm to 454 nm when compared to that of in solution, probably due to the changed polarity of PMMA and intermolecular interaction in the solid state.

Low-temperature (77 K) fluorescence (Fl) and phosphorescence (Ph) spectra allowed evaluation of the energies of the singlet (S_1) and triplet (T_1) states, giving a calculated separation of 0.47 eV (Fig. 3c), consistent with the value (0.44 eV) from calculation and emphasising the difficult RISC process. Excited-state lifetimes of ***R*-3** in toluene solution by time-resolved emission (λ_{ex} = 350 nm; Fig. 3d) showed single exponential kinetics with an excited state lifetime of 13.6 ns, similar to that in doped PMMA films (17.5 ns, Fig. S15, ESI†). In conjunction with the large ΔE_{ST}, the materials are evidently fluorescent. PLQY was evaluated at 33.7% for ***R*-3** doped in PMMA film. Data for ***S*-3** are found in Fig. S16 (ESI†).

Clear mirror-image electronic circular dichroism (ECD) signals were detected for ***R*-3** in neat films (Fig. S17, ESI†), while strong mirror-image CPL spectra were observed in neat films at room temperature, demonstrating that integration of the chiral moiety into the chromophore can lead to CPL emission (Fig. 4a and c). Values of the luminescence dissymmetry factor ($|g_{lum}|$) for ***R*/*S*-3** were calculated to be 3.0×10^{-2}, as determined at the maximum emission wavelength.

To determine the effect of liquid-crystallinity on CPL, pristine films of enantiomeric forms of ***R*-3** were annealed, giving remarkably enhanced CPL signals for the resulting films at room temperature. The values of $|g_{lum}|$ are amplified to 0.131 for ***R*-3**, almost an order of magnitude greater than those obtained for the pristine film. This amplification most likely has its origin in the larger domain sizes that result from annealing.[29] To further verify the chiroptical properties, the rotation-angle-dependent CPL spectra were measured for pristine films (Fig. S18, ESI†) and show only minor change with rotation angle, suggesting strongly

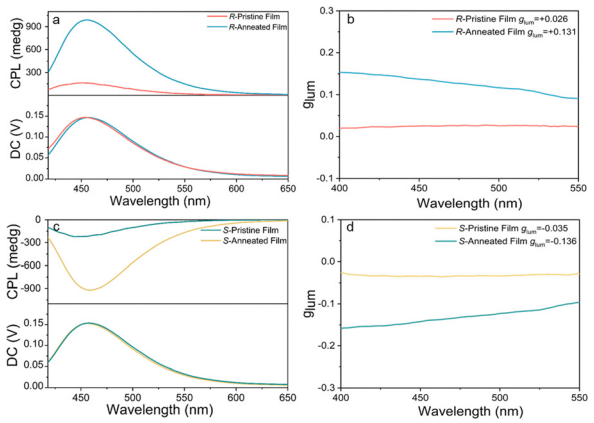

Fig. 4 (a) CPL spectra and (b) g_{lum} values of CPL *versus* wavelength of ***R*-3** in neat films; (c) CPL spectra and (d) g_{lum} values of CPL *versus* wavelength of ***S*-3** in neat films (the annealing temperature was 160 °C).

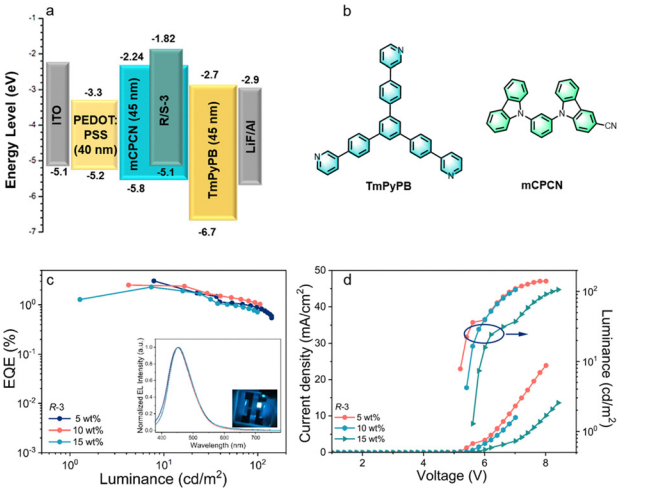

Fig. 5 Device data for ***R*-3**: (a) the device configuration; (b) chemical structure of the host (mCPCN) and electron-transporting material (TmPyPB); (c) curves of external quantum efficiency (EQE) value *versus* luminance; (d) curves of current density–voltage–luminance (*J*–*V*–*L*).

that the chiroptical property is intrinsic. As such, the combination of liquid crystallinity with circularly polarised emission evidently represents a very promising route for the development of effective CPL emitters.

The electroluminescent (EL) properties of the chiral emitters were investigated by fabricating solution-processed OLEDs with the configuration of ITO/PEDOT: PSS (40 nm)/mCPCN: *x* wt%***R*-3/*S*-3** (5, 10, 15 wt%, 45 nm)/TmPyPB (45 nm)/LiF (0.5 nm)/Al (120 nm). The device configuration and the chemical structures of the materials in the device are shown in Fig. 5 (Fig. S19 for ***S*-3**, ESI†), and the EL data are collected in Table S2 (ESI†).

As shown in Fig. 5c inset, the ***R*-3**-based devices show blue emission at 455 nm, analogous with the molecular PL profile and implying that the emission in the device originates from the intrinsic emitter. Correspondingly, the CIE (Commission Internationale de L'Eclairage) coordinates are (0.16, 0.15), with the current density–voltage-luminance (*J*–*V*–*L*) curves of the devices showing a relatively large turn-on voltage ($V_{turn\text{-}on}$: at 1 cd m^{-2}) of 5.5 V. Crucially, there is a negligible effect on the EL spectra when the dopant concentration is increased, probably due to suppressed intermolecular interactions on account of the twisted molecular geometry. As only singlet excitons are harvested, reasonable performance with a maximum EQE of 2.5%, a current efficiency (CE) of 2.74 cd A^{-1} and a luminance (*L*) of 105.8 cd m^{-2} was achieved for the ***R*-3**-based devices. Unfortunately, it did not prove possible to observe CPEL from these devices, which we attribute primarily to the absence of a mesophase as the dopant concentration is too low.

In conclusion, luminescent, enantiomeric liquid-crystalline materials ***R*/*S*-3** were prepared by attaching a suitable chromophore and mesogenic units to the periphery of a chiral binaphthol. The distribution of the frontier orbitals of the molecule demonstrate that the chiral unit is involved the fluorescence, leading to the observation of luminescence dissymmetry and the compounds were found to emit in the blue part of the

spectrum. The materials showed a stronger fluorescence, leading to the observation of luminescence dissymmetry and the compounds were found to emit in the blue part of the spectrum. The materials showed a higher-temperature SmA* phase, below which was a bilayer SmA_2*phase that persisted down to room temperature owing to supercooling. Symmetric circular dichroism and circularly polarised luminescence signals were observed for ***R*/*S*-3** in the solid state, with annealed films showing a much-amplified g_{lum} value of up to 0.13 compared to the pristine film. This is interpreted as arising from the formation of larger domains which will act to reduce scattering. However, while the modest efficiency of the molecular photoluminescence led to equally modest external quantum efficiency for the OLED device of 2.5%, it was observed that the rather three-dimensional nature of the mesogenic chromophore meant that there was no observable concentration quenching as a function of emitter concentration. This is in contrast what is observed commonly where it is expected that efficiency will fall off with increasing emitter concentration as a result of self-quenching. This therefore suggests that the use of emissive materials that are less prone to self-assembly is an attractive design strategy for new chromophoric systems. In particular, liquid crystals with twisted geometries are a potentially fertile area for future development of materials with high luminescence dissymmetry.

Financial support was from the National Natural Science Foundation of China (no. 22371020, 52073035, U1663229), the special program for foreign talents in Changzhou City (CQ20224052) and the University of York. The authors also thank the Analysis and Testing Center, NERC Biomass of Changzhou University for their help with NMR measurements, and Binghong He and Xuefeng Yang for discussion of the device and chiroptical properties of the materials.

Conflicts of interest

There are no conflicts to declare.

Notes and references

‡ Properties are reported in the text for one enantiomer, with data for the other enantiomer in the ESI.† Properties are identical unless noted otherwise.

1 L. Frédéric, A. Desmarchelier, L. Favereau and G. Pieters, *Adv. Funct. Mater.*, 2021, **31**, 2010281.
2 D.-W. Zhang, M. Li and C.-F. Chen, *Chem. Soc. Rev.*, 2020, **49**, 1331–1343.
3 G. Albano, G. Pescitelli and L. Di Bari, *Chem. Rev.*, 2020, **120**, 10145–10243.
4 G. Meng, J. Zhou, X. S. Han, W. Zhao, Y. Zhang, M. Li, C. F. Chen, D. Zhang and L. Duan, *Adv. Mater.*, 2023, 202307420.
5 Z. Qin, T. Wang, H. Gao, Y. Li, H. Dong and W. Hu, *Adv. Mater.*, 2023, **35**, 2301955.
6 L. Wan, Y. Liu, M. J. Fuchter and B. Yan, *Nat. Photonics*, 2022, **17**, 193–199.
7 X. Wu, X. Yan, Y. Chen, W. Zhu and P.-T. Chou, *Trends Chem.*, 2023, **5**, 734–747.
8 S. H. Chen, D. Katsis, A. W. Schmid, J. C. Mastrangelo, T. Tsutsui and T. N. Blanton, *Nature*, 1999, **397**, 506–508.
9 K. L. Woon, M. O'Neill, G. J. Richards, M. P. Aldred, S. M. Kelly and A. M. Fox, *Adv. Mater.*, 2003, **15**, 1555–1558.
10 M. Gon, R. Sawada, Y. Morisaki and Y. Chujo, *Macromolecules*, 2017, **50**, 1790–1802.
11 F. Zinna, G. Albano, A. Taddeucci, T. Colli, L. A. Aronica, G. Pescitelli and L. Di Bari, *Adv. Mater.*, 2020, **32**, 202002575.
12 Y.-F. Wang, M. Li, J.-M. Teng, H.-Y. Zhou, W.-L. Zhao and C.-F. Chen, *Angew. Chem., Int. Ed.*, 2021, **60**, 23619–23624.
13 P. Fan, Z. Fang, S. Wang, Q. Dong, C. Xiao, A. J. McEllin, D. W. Bruce, W. Zhu and Y. Wang, *Chin. Chem. Lett.*, 2023, **34**, 1001–8417.
14 L. Frédéric, A. Desmarchelier, L. Favereau and G. Pieters, *Adv. Funct. Mater.*, 2021, **31**, 2010281.
15 K. Watanabe, H. Iida and K. Akagi, *Adv. Mater.*, 2012, **24**, 6451–6456.
16 G. Qian, X. Yang, X. Wang, J. D. Herod, D. W. Bruce, S. Wang, W. Zhu, P. Duan and Y. Wang, *Adv. Opt. Mater.*, 2020, **8**, 200775.
17 Z. Chen, C. Zhong, J. Han, J. Miao, Y. Qi, Y. Zou, G. Xie, S. Gong and C. Yang, *Adv. Mater.*, 2022, **34**, 2109147.
18 S.-J. Liu, L. Zhu, Y.-H. Zhang, W. Chen, D. Zhu, P. Chen and Y.-Q. Lu, *Adv. Mater.*, 2023, **35**, 2301714.
19 P. Chen, L.-L. Ma, W. Duan, J. Chen, S.-J. Ge, Z.-H. Zhu, M.-J. Tang, R. Xu, W. Gao, T. Li, W. Hu and Y.-Q. Lu, *Adv. Mater.*, 2018, **30**, 1705865.
20 K. Akagi, T. Yamashita, K. Horie, M. Goh and M. Yamamoto, *Adv. Mater.*, 2020, **32**, 1906665.
21 S. Yamakawa, K. Wada, M. Hidaka, T. Hanasaki and K. Akagi, *Adv. Funct. Mater.*, 2019, **29**, 1806592.
22 Y. Wu, L. H. You, Z.-Q. Yu, J.-H. Wang, Z. Meng, Y. Liu, X.-S. Li, K. Fu, X.-K. Ren and B. Z. Tang, *ACS Mater. Lett.*, 2020, **2**, 505–510.
23 K. Akagi, T. Yamashita, K. Horie, M. Goh and M. Yamamoto, *Adv. Mater.*, 2020, **32**, 1906665.
24 Q. Dong, C. Xiao, B. He, X. Yang, S. Zeng, Q. Zhong, P. Duan, W. Zhu and Y. Wang, *Chem. Commun.*, 2023, **59**, 1473–1476.
25 Y. Yang, N. Li, J. Miao, X. Cao, A. Ying, K. Pan, X. Lv, F. Ni, Z. Huang, S. Gong and C. Yang, *Angew. Chem., Int. Ed.*, 2022, **61**, e202202227.
26 H. Shi, J. Yuan, X. Dong and F. Cheng, *Spectrochim. Acta, Part A*, 2014, **133**, 501–508.
27 X. Zeng, K.-C. Pan, W.-K. Lee, S. Gong, F. Ni, X. Xiao, W. Zeng, Y. Xiang, L. Zhan, Y. Zhang, C.-C. Wu and C. Yang, *J. Mater. Chem. C*, 2019, **7**, 10851–10859.
28 H. D. Arbelo-López, A. D. Rodriguez-Mackenzie, E. M. Roman-Morales, T. Wymore and J. López-Garriga, *J. Phys. Chem. B*, 2018, **122**, 4947–4955.
29 L. Frédéric, A. Desmarchelier, R. Plais, L. Lavnevich, G. Muller, C. Villafuerte, G. Clavier, E. Quesnel, B. Racine, S. Meunier-Della-Gatta, J.-P. Dognon, P. Thuéry, J. Crassous, L. Favereau and G. Pieters, *Adv. Funct. Mater.*, 2020, **30**, 2004838.